Soft impurity walls and Weyl-arc transfer in a superconducting two-dimensional SSH model

Henry Sheehy[1, 2]

[1] School of Physical Sciences, University of Kent, Canterbury CT2 7NH, United Kingdom
[2] QuantaLumin

(Dated: June 16, 2026)

We study a superconducting two-dimensional extension of the Su–Schrieffer–Heeger model in which a finite impurity wall is used as a tunable internal boundary. The clean model is a stack of momentum-resolved SSH chains; after imposing an inter-sublattice pairing field it supports Majorana-arc boundary modes in the same symmetry setting as the Weyl-SSH construction of Rosenberg and Manousakis. Here the boundary is not introduced by cutting the system open. Instead, a one-cell-thick onsite potential wall is grown inside a periodic torus, with wall length ℓ and strength V controlling the crossover from a soft defect to a hard internal boundary. In the imposed-pairing problem, tracking the same wall-projected Bogoliubov-de Gennes branch by eigenvector overlap shows a sharp transfer of the $k_y = 0$ arc mode from the bulk continuum toward the near-zero hard-wall branch. We define a scalar order parameter $\Psi_{\rm arc}(V)$ from this tracked branch and find a finite-size critical form consistent with a soft-to-hard boundary quantum transition. We then relax the pairing field with a self-consistent mean-field calculation. The wall does not simply scatter quasiparticles: it suppresses the local Gor'kov field and expels $|\Delta_{AB}|$ from the wall while leaving the off-wall condensate finite. The combined result is a controlled route from clean momentum-space topology to a real-space, tunable boundary in a microscopic superconducting SSH lattice.

I. INTRODUCTION

The one-dimensional SSH model is the canonical example of a chiral topological band problem with boundary zero modes [1]. Its two-dimensional extensions are useful because each transverse momentum can behave as a separate SSH chain, so the boundary spectrum records how a family of one-dimensional invariants evolves through momentum space [2, 3]. When such a system is paired, the Bogoliubov-de Gennes (BdG) problem can host Majorana boundary arcs connecting projected Weyl nodes [4–8].

The practical question addressed here is not whether a clean open boundary has an arc. Instead, we ask whether a local impurity wall inside a periodic system can continuously become an internal boundary and carry the same arc physics. This is the natural finite-device question for a soft boundary: the system begins as a torus, the wall is a microscopic perturbation, and only at large wall strength should it behave like a cut. The central result is that the wall strength controls a visible transfer of a tracked Weyl-arc branch from a bulk-scale excitation to the near-zero hard-wall branch. Self-consistency changes the interpretation but not the basic picture: the wall also suppresses the anomalous field, so a strong wall is a boundary in the mean-field texture as well as in the single-particle Hamiltonian.

II. MODEL

We use spinless fermions on a square lattice of unit cells $r = (x, y)$, with two orbitals or sublattices A and B in each cell. The normal-state Hamiltonian is

$$\begin{aligned} H_0 = &-\sum_r \left[v\, c_r^{A\dagger} c_r^B + w\, c_r^{A\dagger} c_{r-\hat{x}}^B + \text{h.c.}\right] \\ &- \sum_{r,s=\pm 1} \left[t_d\, c_r^{B\dagger} c_{r+s\hat{y}}^A - t_d\, c_r^{B\dagger} c_{r+\hat{x}+s\hat{y}}^A + \text{h.c.}\right] \\ &+ \sum_{r,\alpha=A,B} (\epsilon^\alpha - \mu) n_r^\alpha. \end{aligned} \tag{1}$$

For a translation-invariant torus this becomes

$$H_0(\boldsymbol{k}) = -\boldsymbol{h}(\boldsymbol{k}) \cdot \boldsymbol{\sigma} + (\bar{\epsilon} - \mu)\sigma_0, \tag{2}$$

with

$$h_x = v_1(k_y) + w_1(k_y) \cos k_x, \tag{3}$$
$$h_y = w_1(k_y) \sin k_x, \tag{4}$$
$$h_z = \delta\epsilon, \tag{5}$$

where $v_1(k_y) = v + 2t_d \cos k_y$, $w_1(k_y) = w + 2t_d \cos k_y$, $\bar{\epsilon} = (\epsilon^A + \epsilon^B)/2$, and $\delta\epsilon = (\epsilon^B - \epsilon^A)/2$.

The imposed-pairing BdG problem uses an onsite inter-sublattice pair field within each unit cell,

$$H_\Delta = \sum_{x,y} \left[\Delta_0 c_{x,y}^A c_{x,y}^B + \Delta_0^* c_{x,y}^{B\dagger} c_{x,y}^{A\dagger}\right], \tag{6}$$

written in the Nambu basis $\Psi_{\boldsymbol{k}} = (c_{\boldsymbol{k}}^A, c_{\boldsymbol{k}}^B, c_{-\boldsymbol{k}}^{A\dagger}, c_{-\boldsymbol{k}}^{B\dagger})^T$. The central wall protocol adds

$$H_V = V \sum_{(x,y)\in W_\ell} \sum_{\alpha=A,B} n_{x,y}^\alpha, \tag{7}$$

where W_ℓ is a one-cell-thick support of length ℓ. All real-space figures use centered unit-cell coordinates, so the

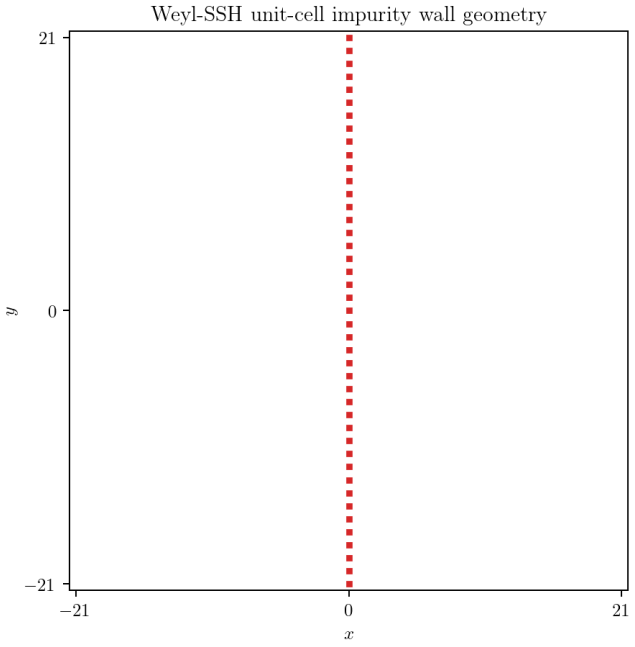

FIG. 1. Soft-wall geometry. The calculation starts from a periodic two-sublattice torus and adds a one-cell-thick impurity wall on a support W_ℓ. The highlighted cells are the wall support, and each highlighted cell contains both A and B sites. Increasing V and ℓ turns the local defect into an effective internal boundary without first imposing open boundary conditions.

plotted wall is at the center of the unit-cell coordinate system. Unless stated otherwise, real-space densities are cell-resolved sums over the A and B sites in each unit cell; pairing-field plots show the inter-sublattice cell field $|\Delta_{AB}(r)|$.

III. CLEAN TOPOLOGICAL SLICES

For $\delta\epsilon = 0$, each fixed k_y slice is a chiral one-dimensional SSH Hamiltonian along x. The off-diagonal block is

$$q(k_x; k_y) = v_1(k_y) + w_1(k_y)e^{-ik_x}, \tag{8}$$

and the slice winding is

$$\nu(k_y) = \frac{1}{2\pi}\Delta_{k_x} \arg q(k_x; k_y). \tag{9}$$

Thus $\nu(k_y) = 1$ when $|w_1(k_y)| > |v_1(k_y)|$ and zero otherwise. The Weyl-SSH construction is the statement that the gap closings between these slices become the endpoints of boundary arcs after pairing [8].

IV. FIXED-PAIRING SOFT-WALL TRANSITION

The imposed-Δ_0 calculation isolates the quasiparticle boundary problem. We use the fixed pairing amplitude $\Delta_0 = 0.3$ and first set $\mu = \delta\epsilon = 0$. For representative wall strengths, the wall-projected spectral function $A(k_y, E)$ shows the boundary branch detach from the bulk response and approach the near-zero hard-wall arc. The viewer-exported panels in Fig. 4 include the tracked branch overlay, making the transfer visible at the scale of the printed figure.

To quantify this transfer, we track the same BdG branch rather than selecting a new local minimum at each parameter point. At a given V, we diagonalize the fixed-k_y BdG strip, seed the wall-weighted positive-energy mode near $k_y = 0$, and continue it through k_y using maximal eigenvector overlap. The resulting branch is the red curve in Fig. 5. This method turns the visually identified arc into a reproducible object.

The $k_y = 0$ point of this tracked branch provides a scalar diagnostic of the wall-driven transfer. Let $\epsilon_{\rm arc}(0; V)$ be the tracked-branch energy at $k_y = 0$. We normalize the finite-size order parameter as

$$\Psi_{\rm arc}(V) = \frac{|\epsilon_{\rm arc}(0; V) - \epsilon_{\rm arc}(0; 0)|}{|\epsilon_{\rm arc}(0; \infty) - \epsilon_{\rm arc}(0; 0)|}. \tag{10}$$

In practice the hard-wall reference is represented by the largest simulated wall strength. The resulting $\Psi_{\rm arc}(V)$ rises from zero to one as the wall becomes a hard internal boundary. The finite-size data are consistent with a critical form

$$\Psi_{\rm arc}(V) \simeq A\left(\frac{V - V_c}{V_c}\right)^{\beta}, \tag{11}$$

with V_c in the few-hopping range. Changing ℓ at fixed weak V mostly transfers spectral weight smoothly, while increasing V for a full wall changes the tracked $k_y = 0$ branch itself. This distinction is why the wall-strength scan is the central transition diagnostic.

The same transfer is visible in real space. The lowest relevant BdG mode is concentrated near the impurity wall and the adjacent periodic boundary cells once the wall is strong. This confirms that the tracked spectral branch is not merely a relabelled bulk eigenvalue.

V. SELF-CONSISTENT WALL FEEDBACK

The imposed-pairing calculation deliberately holds the anomalous field fixed. To test whether the same soft wall survives as a microscopic mean-field feature, we also solve a self-consistent inter-sublattice pairing problem. The interaction is decoupled through the Gor'kov field

$$\kappa_{AB}(r) = \langle c_r^A c_r^B \rangle, \tag{12}$$

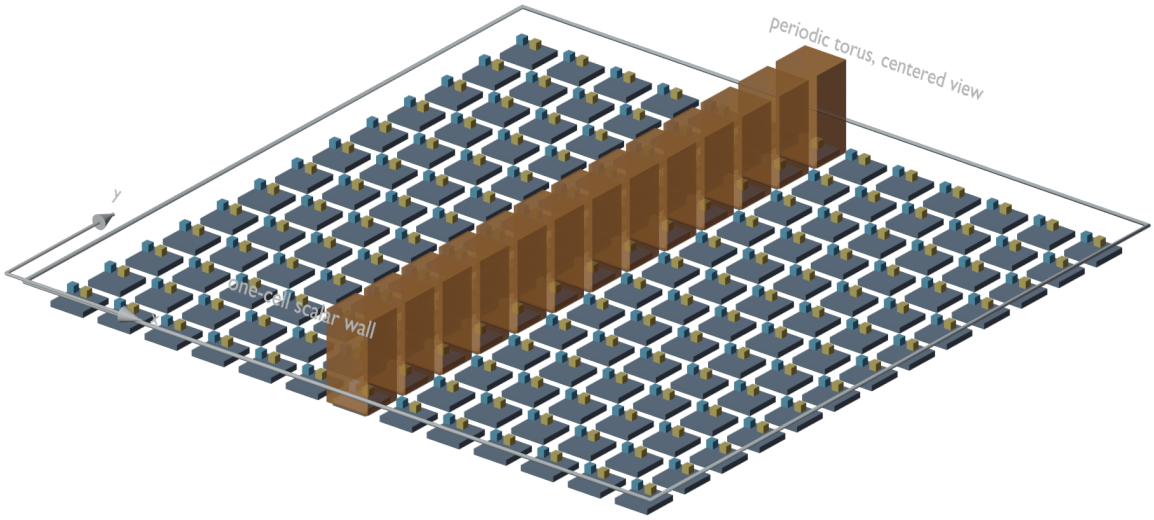

FIG. 2. Three-dimensional view of the same periodic wall setup used in the numerical calculations. The orange cells mark the one-cell-thick scalar wall, the small blue and gold blocks show the two sublattice sites in each unit cell, and the compact axes indicate the centered real-space coordinates used throughout the paper. The transparent render emphasizes that the wall is an internal defect on a periodic torus rather than an imposed open edge.

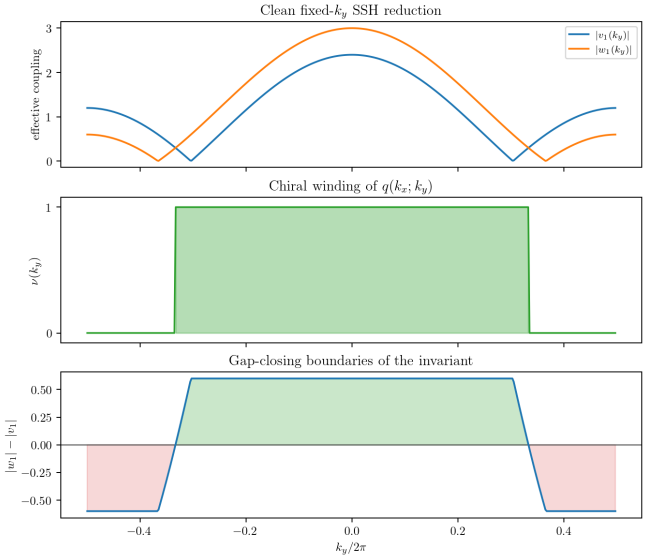

FIG. 3. Clean bulk topology. For $\delta\epsilon = 0$, each k_y slice reduces to a chiral SSH chain along x. The winding changes when the effective intracell and intercell hoppings exchange magnitude. This clean slice invariant predicts where the open-boundary Majorana arc should begin and end; the impurity-wall calculations test whether an internal wall can reproduce that boundary response.

with the local mean-field order parameter

$$\Delta_{AB}(r) = g_{AB}\kappa_{AB}(r). \tag{13}$$

The production calculation uses $g_{AB} = 2.9249$, chosen so the clean off-wall pairing amplitude is comparable to the imposed $\Delta_0 = 0.3$ reference. The fixed-point iteration uses linear mixing,

$$\Delta_{AB}^{(n+1)} = (1-\eta)\Delta_{AB}^{(n)} + \eta\,\Delta_{AB}^{\mathrm{new},(n)}, \tag{14}$$

where η is the weight of the new update.

Table I summarizes the main self-consistent amplitudes. The wall mean falls by more than an order of magnitude over the simulated range, while the off-wall mean remains close to the clean scale. Attempts to fit the wall mean to the same finite-V_c critical form as the fixed-Δ_0 arc are unstable. A simpler interpretation is that SCMFT replaces the sharp imposed-Hamiltonian transfer by an algebraic depletion tail, $|\Delta_{AB}|_{\mathrm{wall}} \sim (V - V_0)^{-\beta}$ with $\beta \simeq 0.7$ over the simulated interval. This is a separate physical effect: the boundary condition is now partly generated by the suppression of the anomalous field itself.

VI. LOCAL MARKER AND SYMMETRY CONTROLS

The clean winding invariant is exact only in the chiral slices of the translation-invariant model. The scalar

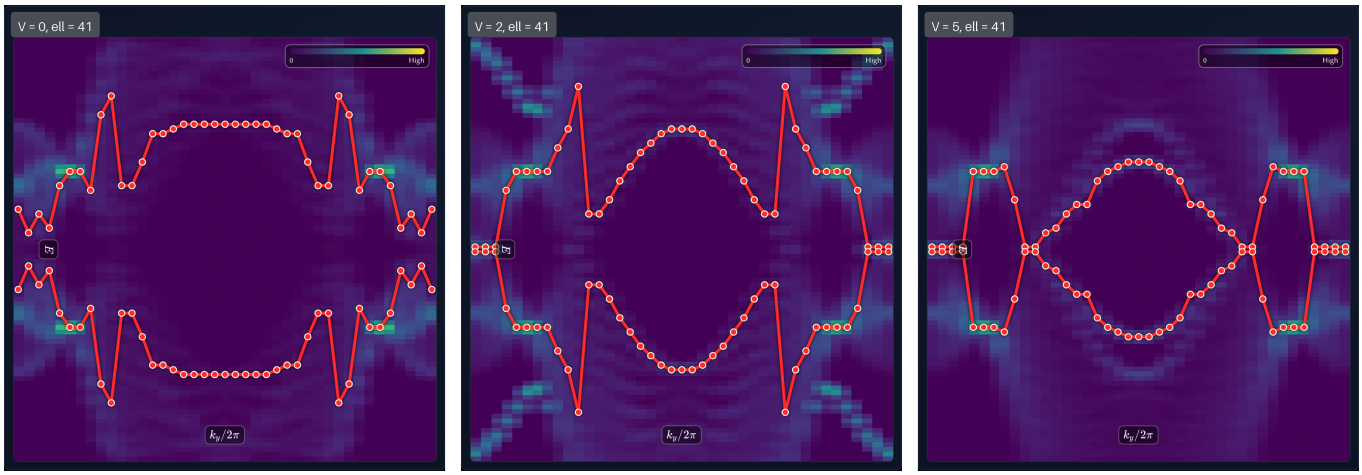

FIG. 4. Viewer-exported wall-strength spectra for the imposed-pairing model on 41×41 unit cells. The panels show $A(k_y, E)$ at $\Delta_0 = 0.3$, $\mu = \delta\epsilon = 0$, and $\ell = 41$. The red curve is the tracked wall branch overlaid directly from the interactive diagnostic. At weak V, the wall-projected spectrum resembles the bulk response. At intermediate V, the boundary branch starts to separate from the continuum. At strong V, the wall acts as an internal hard boundary and the near-zero arc is visible.

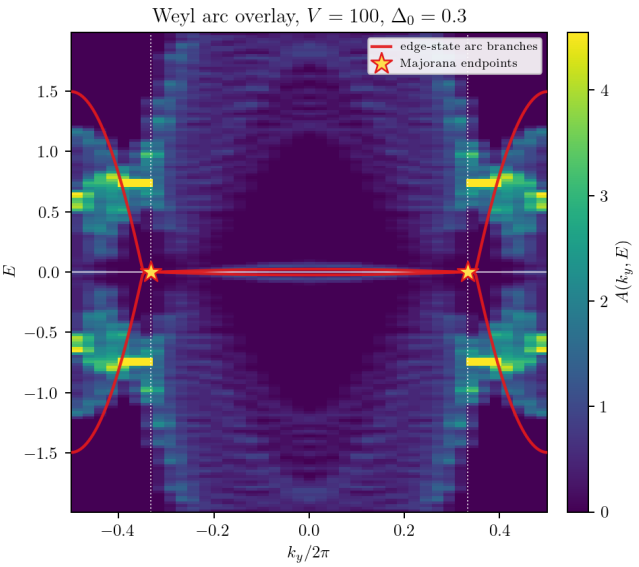

FIG. 5. Tracked Weyl arc on top of the wall-projected spectrum. The background is $A(k_y, E)$. The red curve is a BdG eigenmode branch continued through k_y by eigenvector overlap, and the yellow stars mark the clean Majorana endpoints at $k_y/2\pi = \pm1/3$. The line representation is important: the calculation follows one continuous branch rather than plotting unrelated spectral maxima.

onsite wall in Eq. (7) is a local chiral-symmetry-breaking perturbation because it contributes a same-sublattice onsite term on the wall cells. This does not invalidate the wall-transfer calculation; it clarifies what is being tested. The bulk away from the wall remains governed by the chiral SSH structure, while the wall locally breaks that symmetry and acts as a boundary-forming perturbation.

We use a local chiral marker as a diagnostic rather than

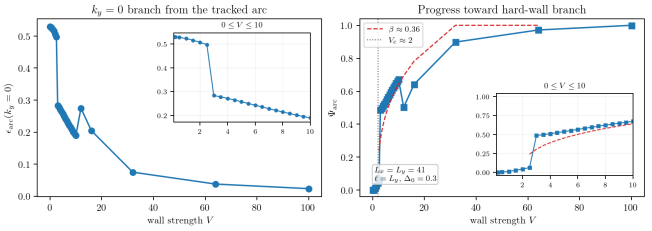

FIG. 6. Fixed-Δ_0 arc-transfer diagnostic. The left panel shows the tracked $k_y = 0$ arc energy as V is increased. The right panel shows the normalized order parameter $\Psi_{\rm arc}(V)$ from Eq. (10). The calculation uses a full wall on a 21×21 unit-cell device with $\Delta_0 = 0.3$. The branch is bulk-scale at weak impurity strength and is pushed down toward the near-zero hard-wall state as the wall becomes strong.

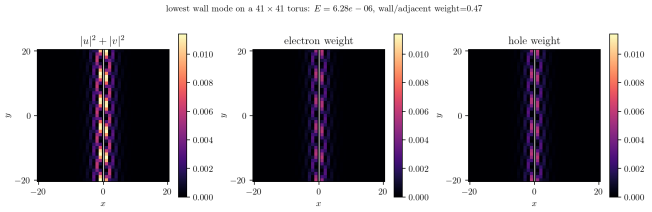

FIG. 7. Real-space density of the low-energy wall mode on 41×41 unit cells. The plotted density is the cell-summed BdG mode weight over A and B sites. Centered coordinates place the wall at the middle of the panel. The low-energy state carries weight near the impurity support and its nearest periodic partners, showing that the wall reorganizes boundary-like modes rather than only shifting a delocalized bulk level.

as a final quantized invariant,

$$\nu_{\rm loc}(r) = -\frac{1}{2}\mathrm{tr}_{A,B\in r}\left[\Gamma Q[X, Q]\right], \qquad (15)$$

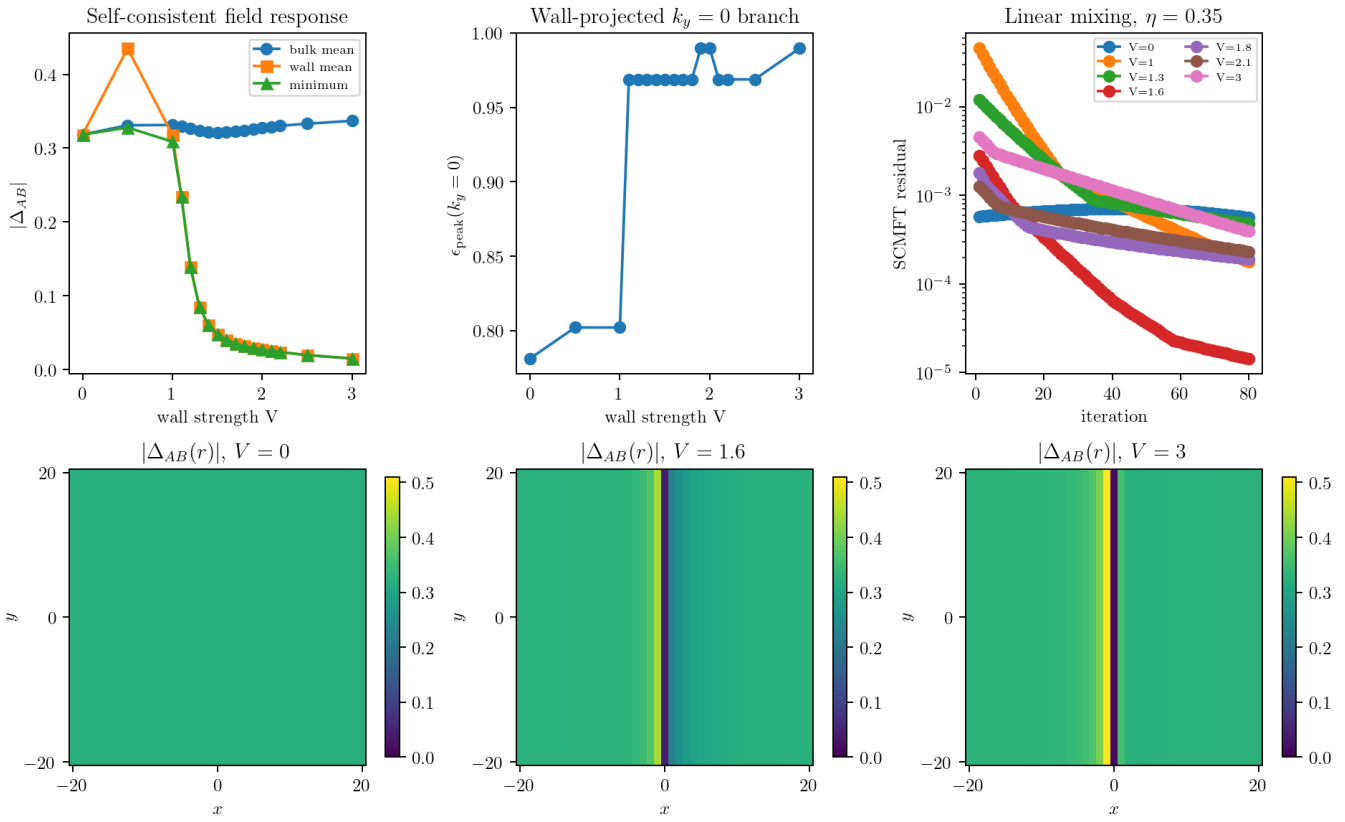

FIG. 8. Self-consistent mean-field wall response. The upper panels track the bulk mean, wall mean, and minimum of $|\Delta_{AB}(r)|$, the corresponding $k_y = 0$ wall branch, and the mixed residual histories. The lower panels show the real-space inter-sublattice field $|\Delta_{AB}(r)|$. The wall is not only a quasiparticle scatterer: it suppresses the local Gor'kov field and expels the pairing amplitude from the wall support. The off-wall condensate remains finite, while the wall-local field decreases rapidly with V.

TABLE I. Self-consistent pairing amplitudes for the wall-stability scan. The wall mean is the average of $|\Delta_{AB}(r)|$ on the impurity support; the off-wall mean excludes the support.

V	$\lvert\Delta_{AB}\rvert_{\rm wall}$	$\lvert\Delta_{AB}\rvert_{\rm bulk}$
1.0	0.318	0.331
1.1	0.234	0.329
1.2	0.139	0.326
1.3	0.0846	0.324
1.5	0.0480	0.321
2.0	0.0271	0.327
3.0	0.0150	0.337

where $\Gamma = +1$ on A, $\Gamma = -1$ on B, and $Q = 1-2P_-$ is the flattened occupied-state projector. The accompanying chiral-breaking diagnostic is

$$\chi_{\rm break} = \frac{\|\{\Gamma, H\}\|}{\|H\|}. \tag{16}$$

VII. DISCUSSION

The fixed-Δ_0 and SCMFT calculations tell complementary parts of the same story. In the fixed-pairing model, the Hamiltonian is controlled enough that one can track a BdG eigenbranch through k_y and measure a scalar order parameter for the soft-to-hard boundary transition. This is the cleanest statement of the Weyl-arc transfer: the $k_y = 0$ branch begins as a bulk-scale spectral feature and moves toward the near-zero hard-wall branch as V grows.

In the self-consistent model, the wall has an additional channel. It suppresses $\kappa_{AB}(r)$ and therefore $\Delta_{AB}(r)$ on the wall support, while the off-wall condensate remains finite. This means that the wall is not just a probe of a pre-existing BdG spectrum. It changes the mean-field problem itself by creating a narrow region where the anomalous field is expelled. The resulting behavior is better described as wall-local depletion with an algebraic tail than as the same finite-V_c arc transition seen in the imposed-pairing model.

The conservative conclusion is that a finite impurity wall in a two-dimensional superconducting SSH lattice can be promoted into an effective internal boundary. The

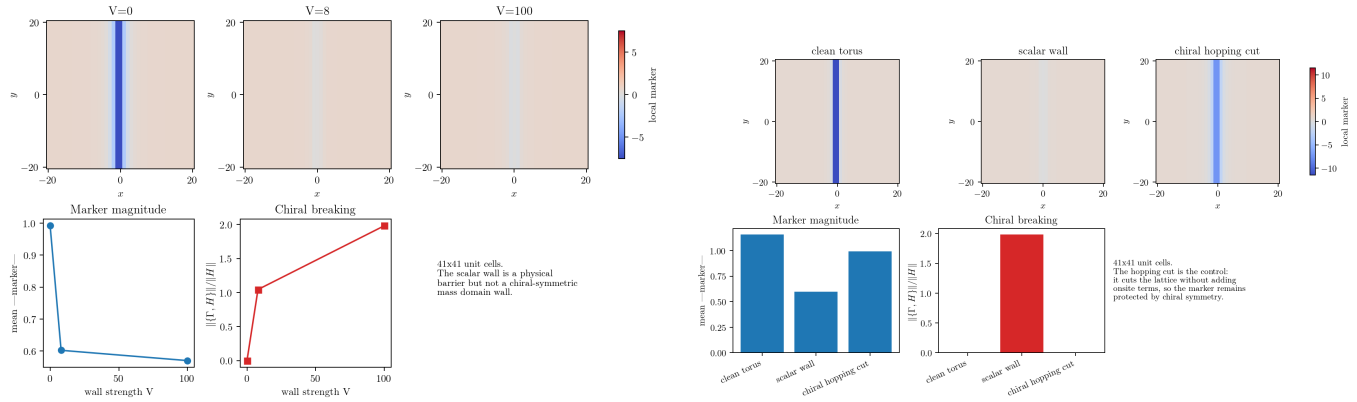

FIG. 9. Local marker and symmetry control on 41×41 unit cells. Left: local marker for the scalar onsite wall. The bulk retains the clean chiral SSH structure, but the onsite impurity wall is a local chiral-symmetry-breaking defect. The marker therefore acts as a diagnostic of how the wall disrupts the local topological texture, not as a proof of an exactly quantized inhomogeneous invariant. Right: the chiral hopping cut is the control; it changes inter-sublattice hopping terms rather than adding onsite potentials. The comparison shows that a scalar wall and a chiral-symmetric cut are distinct boundary mechanisms. The soft-wall results should therefore be read as an impurity-induced internal boundary, not as an ideal chiral-domain-wall invariant.

evidence is a linked chain: clean slice winding, slab Majorana arcs, wall-projected spectral evolution, eigenvector-continuous arc tracking, real-space mode localization, and a self-consistent suppression of the wall pairing field. What remains for a sharper claim is a fully quantized real-space invariant for the inhomogeneous BdG wall, or an explicit disorder and size-scaling analysis showing that the tracked arc and SCMFT depletion survive outside the current finite-device regime.

ACKNOWLEDGMENTS

I thank Jorge Quintanilla for discussions and for suggesting the central idea behind this study. I also thank Sam Carr, Gunnar Möller, and the wider PQM group at the University of Kent for useful discussions. Numerical data and figures were generated with the `qulab.research.ssh_2d` module in QuLab [9].

[1] W. P. Su, J. R. Schrieffer, and A. J. Heeger, Solitons in polyacetylene, Physical Review Letters **42**, 1698 (1979).
[2] B.-H. Chen, *Two-Dimensional Extended Su–Schrieffer–Heeger Model*, Master's thesis, National Taiwan Normal University (2018).
[3] C.-A. Li, Topological states in two-dimensional su-schrieffer-heeger models, Frontiers in Physics **10**, 861242 (2022).
[4] A. P. Schnyder, S. Ryu, A. Furusaki, and A. W. W. Ludwig, Classification of topological insulators and superconductors in three spatial dimensions, Physical Review B **78**, 195125 (2008).
[5] S. Ryu, A. P. Schnyder, A. Furusaki, and A. W. W. Ludwig, Topological insulators and superconductors: tenfold way and dimensional hierarchy, New Journal of Physics **12**, 065010 (2010).
[6] A. Y. Kitaev, Unpaired majorana fermions in quantum wires, Physics-Uspekhi **44**, 131 (2001).
[7] N. Read and D. Green, Paired states of fermions in two dimensions with breaking of parity and time-reversal symmetries and the fractional quantum hall effect, Physical Review B **61**, 10267 (2000).
[8] P. Rosenberg and E. Manousakis, Topological superconductivity in a two-dimensional weyl ssh model, arXiv:2203.12004 (2022), arXiv:2203.12004 [cond-mat.supr-con].
[9] H. Sheehy, Qulab research module for two-dimensional ssh soft walls (2026), repository module: qulab.research.ssh_2d.